THE JOURNAL OF PHYSICAL CHEMISTRY Letters

Letter

Cite This: J. Phys. Chem. Lett. 2018, 9, 3057−3061

pubs.acs.org/JPCL

Surface Ligand Promotion of Carbon Dioxide Reduction through Stabilizing Chemisorbed Reactive Intermediates

Zhijiang Wang,*[†,‡] Lina Wu,[⊥] Kun Sun,[†] Ting Chen,[∥] Zhaohua Jiang,[†,‡] Tao Cheng,*[§] and William A. Goddard, III*[§]

[†]State Key Laboratory of Urban Water Resource and Environment, and [‡] School of Chemistry and Chemical Engineering, Harbin Institute of Technology, Harbin 150001, China

[⊥]Molecular Imaging Research Center of Harbin Medical University, the Fourth Hospital of Harbin Medical University, Harbin 150001, China

[∥]Department of Chemistry, University of Oxford, South Parks Road, Oxford OX1 3QR, United Kingdom

[§]Materials and Process Simulation Center (MSC) and Joint Center for Artificial Photosynthesis (JCAP), California Institute of Technology, Pasadena, California 91125, United States

Supporting Information

ABSTRACT: We have explored functionalizing metal catalysts with surface ligands as an approach to facilitate electrochemical carbon dioxide reduction reaction (CO_2RR). To provide a molecular level understanding of the mechanism by which this enhancement occurs, we combine *in situ* spectroscopy analysis with an interpretation based on quantum mechanics (QM) calculations. We find that a surface ligand can play a critical role in stabilizing the chemisorbed CO_2, which facilitates CO_2 activation and leads to a 0.3 V decrease in the overpotential for carbon monoxide (CO) formation. Moreover, the presence of the surface ligand leads to nearly exclusive CO production. At −0.6 V (versus reversible hydrogen electrode, RHE), CO is the only significant product with a faradic efficiency of 93% and a current density of 1.9 mA cm^{-2}. This improvement corresponds to 53-fold enhancement in turnover frequency compared with the Ag nanoparticles (NPs) without surface ligands.

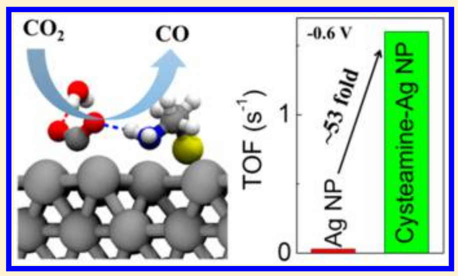

Directly using CO_2 as carbon-based fuel feedstock is promising for developing a sustainable carbon-based economy, which, could also reduce the impact of CO_2 on climate change.[1−9] Electroreduction of CO_2 to CO is of particular importance due to the central role of CO in reducing CO_2 to hydrocarbon fuels. Although the redox potential of CO_2 to CO is only −0.11 V (vs RHE, hereafter all potentials referenced to RHE), activation of CO_2 always requires significant overpotential due to its inertness.[10,11] Until now, the reported performance of CO_2 catalysis remains far from meeting the minimum requirement for large-scale applications. Therefore, it would be useful to develop rational design principles for facilitating improved CO_2RR.

Among transition metals, noble metal Au and Ag exhibit superior performance in reducing CO_2 to CO. Ag is more appealing, considering the lower cost compared with Au. Meanwhile, the excellent mechanical property of Ag (such as high ductility) allows further fabrication to improve the activity and stability. Ag is a promising catalyst for both laboratory applications and future industrial production. Extensive efforts have been devoted to improving CO_2RR performance for Ag-based electrodes, including tuning their defect site, size, shape, and component.[12−21] Jiao et al. reported a nanoporous Ag achieved for 92% selectivity under a potential of −0.6 V.[14] Luo and co-workers developed triangular Ag nanoplates with predominant Ag(100) facets to reach 96.8% selectivity under −0.86 V.[22] As a more facile and efficient approach, surface ligands have been reported to promote CO_2RR. For example, amine-functionalized ligands, cysteamine ($HS-CH_2-CH_2-NH_2$), can significantly improve the CO_2RR with reduced onset potential and 84.4% selectivity for CO formation under −0.75 V. Hwang et al. proposed that this enhancement is due to Ag−S interaction inducing surface localization of the unpaired electron.[13] However, for enzymes of hydrogenase or CO-dehydrogenase, the amino residues can also assist the H_2 or CO_2 absorption and activation by coordinating interactions with closed metal ions.[23,24] Thus, in addition to the electron-dislocation effect reported previously, we suspected that the surface ligands could also stabilize chemisorbed CO_2 geometrically. Herein, we employed QM to investigate the CO_2RR on Ag with an attached cysteamine ligand to stabilize the process of physisorbed CO_2 to chemisorbed CO_2.

In our QM simulations, we employed a four-layer 3 × 3 Ag(111) surface, with one or two cysteamine molecules chemisorbed to the surface via Ag−S bonds, corresponding to a surface concentration of 1/9 ML to 2/9 ML. We placed 32

Received: March 28, 2018
Accepted: May 22, 2018
Published: May 22, 2018

DOI: 10.1021/acs.jpclett.8b00959
J. Phys. Chem. Lett. 2018, 9, 3057−3061

water molecules on the surface forming five layers of explicit water to simulate the electrolyte/electrode interface.

One CO_2 molecule was inserted, and after 20 ps of ab initio molecular dynamics (AIMD) simulations we found that the average distance between CO_2 (the center of mass) and Ag surface is 3.74 Å, which is a typical range of nonbonded interaction indicating a physisorbed state of CO_2 on Ag surface. Such physisorbed CO_2 on Ag is similar to that we observed on copper (Cu) electrode (3.67 Å).[25,26] In our previous work, we found that the formation of chemisorbed CO_2 from physisorbed CO_2 is the rate-limiting step in CO_2RR to CO.[25] Thus, we applied a constraint force to drive the chemical reactions from physisorbed CO_2 to chemisorbed CO_2 by taking the distance (Z_{CO2}) between CO_2 (the center of mass) and Ag surface as a collective variable (the simulation details are in the Supporting Information). The calculated free energy profiles are shown in Figure 1C. For the pure Ag case, the free energy is

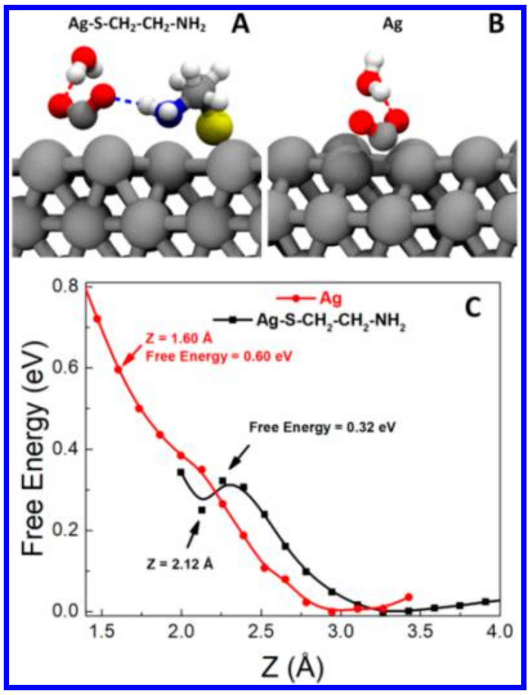

Figure 1. (A) chemisorbed CO_2 on cysteamine functionalized Ag(111) surface. (B) Chemisorbed CO_2 on Ag(111) surface. (C) The free energy profile of the CO_2 approaching surface. Only the water molecules directly forming hydrogen bond are shown (the remaining 31 or 30 solvent water molecules are removed for clarity). The hydrogen bonds are shown as a slashed line. The colors are Ag in silver, C in gray, O in red, N in blue, S in yellow, and H in white.

a minimum at Z = 3 Å, corresponding to a van der Waals or physisorbed state, indicating that chemisorbed CO_2 is not stable on the clean Ag surface. A likely pathway for CO_2 reduction on Ag would be electron-coupled proton transfer to form *COOH, but we expect there to be little chance to capture the chemisorbed CO_2 on Ag surface at the operation potential in CO_2RR. As the applied biasing force is changed continuously, we find that physisorbed CO_2 starts to convert to chemisorbed CO_2 as the distance between CO_2 and the topmost Ag atoms approach 1.60 Å. Instead of a "mixed coordination" as we found on Cu (100),[25] the chemisorbed CO_2 on Ag is in the configuration of "carbon coordination" as shown in Figure 1B. The AIMD simulation shows that there is always one neighbor water molecule forming a hydrogen bond to stabilize the chemisorbed CO_2. At this distance, the free energy is 0.6 eV, indicating that the minimum applied potential to activate CO_2 on Ag(111) is −0.6 V. Thus, this chemisorbed CO_2 remains very unstable, immediately returning to physical adsorbed CO_2 after removing the constraint.

However, in the case of Ag−S−CH_2−CH_2−NH_2 chemisorbed CO_2 is much more stable, especially when the cysteamine forms a cis-configuration on the surface. In this case, the nitrogen (N) atom from cysteamine binds to the surface, preventing protonation of −NH_2 to form −NH_3^+, which is the stable form in bulk solution at this pH condition. As the distance between CO_2 from the surface reaches 2.12 Å (at a distance 0.52 Å more extended than on pure Ag), we find chemisorbed CO_2 as shown in Figure 1A. AIMD simulation snapshot shows that both water and terminal NH_2 group provide hydrogen bond (HB) to chemisorbed CO_2 as shown in Figure 1A. The extra HB due to the cysteamine may further stabilize chemisorbed CO_2. As shown in Figure 1C, the chemisorbed CO_2 is a local minimum in the free energy profile. Thus, it is possible that chemisorbed CO_2 is detectable experimentally as a metastable intermediate. With Ag−S−CH_2−CH_2−NH_2, the free energy for activating CO_2 decrease to 0.32 eV. Thus, we estimate that CO_2 activation on Ag−S−CH_2−CH_2−NH_2 would occur at a 0.28 V less negative onset potential than for pure Ag, consistent with 0.3 V decrease in experiment (as shown in Figure 4).

Previously, such stabilization effects had been rationalized as pure electronic effects arising from the Ag−S interaction.[16] Instead, our AIMD atomic structure analysis reveals that geometric stabilization effect also plays an important role. To elucidate the influence of electron localization and geometry stabilization effect on CO_2RR, we carried out three types of experiments:

- ligand-free Ag NPs
- cysteamine-capped Ag NP (C_2−Ag)
- 11-Amino-1-undecanethiol capped Ag NP (C_{11}−Ag)

Both C_2−Ag and C_{11}−Ag have a similar localization effect, but for C_{11}−Ag the carbon chain is too long to form a complex with chemisorbed CO_2 so that we find no geometry stabilization. All the prepared Ag NPs have a similar core diameter and density distribution on the carbon black support.

Figure 2 illustrates a detailed characterization for C_2−Ag NPs. Transmission electron microscopy (TEM) image (Figure 2A) shows that C_2−Ag NPs have core sizes of ∼10 nm. High-resolution TEM image (Figure 2B) and XRD data (Figure S3) indicate that these NPs possess a face-centered cubic Ag crystal phase. In the X-ray photoelectron spectroscopy (XPS) spectra (Figure 1C), the S $2p_{3/2}$ peak centered at 162.3 eV arises from thiol groups covalently bridged to the silver to form Ag−S−C links. Fourier transformed infrared spectroscopy (FT-IR) spectrum (Figure 1d) confirms the presence of −NH_2 groups on C_2−Ag NPs.[27−29] The detailed characterization for C_{11}−Ag and ligand-free Ag NPs are presented in Supporting Information (Figures S1−S3).

We studied the chemisorption of CO_2 on C_2−Ag NP using *in situ* attenuated total reflectance infrared (ATR-IR) spectroscopy, which was taken at −0.6 V vs RHE in 0.1 M $NaHCO_3$. As the purged gas is changed from Ar as CO_2, the first feature is the peak at 1409 cm^{-1}, attributed to chemisorbed CO_3^{2-} on the Ag surface,[30] which significantly decreases in intensity (Figure 3A), accompanied by two new peaks appearing at 1945 and 2343 cm^{-1}. The adsorption peak at 1945 cm^{-1} stems from

DOI: 10.1021/acs.jpclett.8b00959
J. Phys. Chem. Lett. 2018, 9, 3057−3061

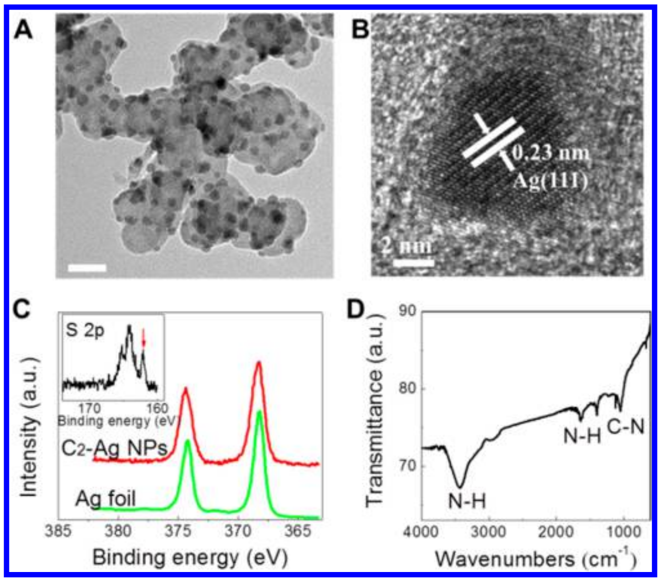

Figure 2. Characterization of C_2−Ag NPs. (A) TEM image (scale bar being 40 nm), (B) HRTEM image, (C) XPS spectrum, inset showing a high-resolution S 2*p* XPS spectrum, and (D) FT-IR spectrum.

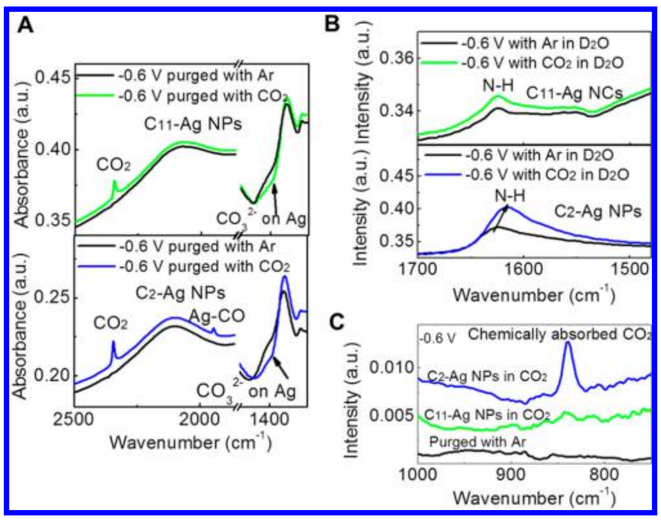

Figure 3. *In situ* ATR-IR spectra of C_2−Ag and C_{11}−Ag NPs at −0.6 V purged with Ar or CO_2. (A,C) the electrolyte is 0.1 M $NaHCO_3$ resolved in H_2O; (B) the electrolyte is 0.1 M $NaHCO_3$ resolved in D_2O. Because the δ_{HOH} bending mode of adsorbed water obscures the information on N−H bond and C═O bending, the experiment using D_2O to replace H_2O was carried out.

chemisorption of the CO reaction intermediate on Ag surface to form Ag−CO.[30,31] The peak of 2343 cm^{-1} is from CO_2. Notably, as presented in Figure 2B, the peak at 1624 cm^{-1}, assigned to −N−H in-plane deformation, is shifted to a lower frequency of 1610 cm^{-1} (Figure 3B). pH has little influence on this peak (Figure S8). Therefore, the ATR-IR peak shift is possibly associated with the appearance of reactive intermediate, in which case chemisorbed CO_2 is the most possible candidate. This shift suggests that there is a chemical interaction between NH_2 and CO_2 as well as the reaction intermediates. The peak locating at ~839 cm^{-1}, attributed to the CO_2 bonding with − NH_2, appears under the applied potential,[32] which further confirms the chemisorbing CO_2 taking place on C_2−Ag NPs during the electrolysis.

By contrast, the Ag−CO intermediate adsorption peak becomes negligible in the cases of C_{11}−Ag NP (Figure 3A) and ligand-free Ag NPs (Figure S4) as the CO_2RR catalysts. The difference on the ATR-IR spectra should be due to the lifetime variation of the intermediates. As presented in Figure 1, the chemically boned intermediates are longer lived on the surface of cysteamine capped Ag NPs, which makes them detectable by ATR-IR. Upon extending the alkyl chain length from C_2 to C_{11}, the long alkyl chain inhibits the simultaneous interaction of CO_2 with Ag and NH_2 groups, because $-NH_2$ in C_{11}−Ag is far away from Ag surface and very possibly protonated to $-NH_3^+$. This is supported by the ATR-IR spectra of C_{11}−Ag NPs in Figure 3B. The NH_2 peak of C_{11}−Ag NPs remains stationary at the electrolysis state. Furthermore, the chemisorbed CO_2 peak at ~839 cm^{-1} is undetectable in C_{11}−Ag NPs. All these suggest that the ligands assisting the chemisorption of CO_2 on Ag catalysts does not occur for C_{11}−Ag NPs.

Figure 4 shows the electrochemical CO_2RR activity of these Ag NPs. CO is the primary product for all three cases. The potential-dependent FEs of CO formation shows that for C_2−Ag NPs, significant amounts of CO are generated at an onset potential of −0.2 V, which is 0.09 V below the theoretical equilibrium potential of CO_2/CO (−0.11 V). The onset potentials for C_{11}−Ag NPs are shifted to −0.3 V. When ligands are removed from the surface, ligand-free Ag NPs require the highest onset potential of −0.5 V. The FE increases as the potential is increased. C_2−Ag NPs are the most active for CO formation with FE reaching 93% at −0.60 V. Extending the alkyl chain length to C_{11} decreases the catalytic performance for CO_2RR. The CO partial current density of different NPs shown in Figure 4B. The electrochemical surface area is determined using lead underpotential deposition (UPD).[33] It can be found that C_2−Ag NPs possess the highest CO partial current density values at same conditions. The order of the catalytic activity for these Ag NPs is C_2−Ag > C_{11}−Ag > ligand-free Ag NPs. Compared to ligand-free Ag NPs, the C_2−Ag NPs can decrease the overpotential by 300 mV at 1 mA cm^{-2}. Taking −0.6 V as a reference potential, the turnover frequency (TOF) of C_2−Ag reaches 1.6 s^{-1}, which is ~10-fold better than that of C_{11}−Ag NPs (0.14 s^{-1}) and 53 times higher than that of ligand-free Ag NPs (0.03 s^{-1}) (Figure 4C). Meanwhile, the ligands possess high stability on Ag NPs even under the negative potential for CO_2RR (Figures S9 and S10).

This evaluation on CO_2RR indicates that thiolate ligands can improve the catalytic activity. However, the significant difference in activity of C_2−Ag and C_{11}−Ag NPs suggests that the electron-localization effect due to the thiolate anchoring on Ag is not sufficient to explain this phenomenon. Our *in situ* ATR-IR combined with QM-based molecular dynamics simulations indicates that the cis form of C_2 can further provide an extra stabilization effect by utilizing the terminal NH_2 forming HB bond with chemisorbed CO_2, which further reduces the overpotential. C_{11} lacks of such ability because the carbon chain is too long leads to a significant hydrophobic nature that forces the ligand to fully extend. Thus, C_{11}−Ag NPs have less activity compared to C_2−Ag, but due to the electron-localization function, it is better than ligand-free Ag NPs. The synergistic combination of the assisted CO_2 chemisorption on Ag catalysts by $-NH_2$ with the electron-localization effect endows the C_2−Ag NPs with superior high activity for CO_2RR compared to reported Ag-based catalysts (Table S1).

DOI: 10.1021/acs.jpclett.8b00959
J. Phys. Chem. Lett. 2018, 9, 3057−3061

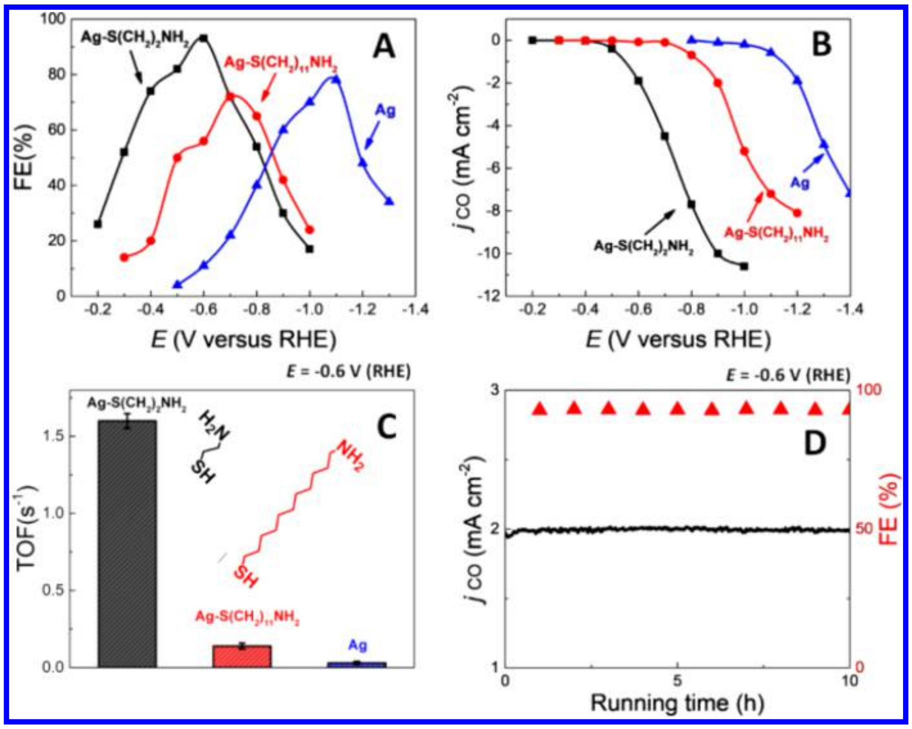

Figure 4. Influence of alkyl chain length on the CO_2 electroreduction catalysis. (A) FE for CO vs potential; (B) CO partial current density vs potential; (C) TOF for CO at −0.6 V; (D) stability of the C_2−Ag NPs characterized by FE for CO and total current density versus time at −0.6 V.

The synthesized C_2−Ag NPs exhibit superior stability in catalytic activity. Its total current density versus time and CO FE versus time at −0.6 V vs RHE remain quite stable even after electrolysis for 10 h (Figure 4D). The TEM image of the C_2−Ag NPs after 10-h electrolysis shows almost no appreciable differences in the morphology (Figure S7).

Most important is that the promotion effect of surface ligands on catalysis is readily applied to enhance the catalysis of Ag foil. We immersed polished Ag foil into dilute cysteamine solution (5×10^{-6} mmol) for 10 min. Consistent with cysteamine on Ag NPs, the cysteamine self-assembled monolayer (SAM) coating on Ag foil enhances the catalytic activity and selectivity of CO_2 (Figure S8), decreasing the overpotential requirement for CO formation and increasing the CO partial current density. This experiment verifies that cysteamine SAM modification is a general approach to improving Ag electrodes for selective electroreduction of CO_2 toward CO.

In summary, our results demonstrate that thiolate SAM ligands can stabilize the chemisorbed CO_2 by geometrically and electron-dislocation effects to improve the catalytic activity of CO_2 electrochemical reduction markedly. Under the synergistic electron-dislocation and geometric CO_2 chemisorption effects, the NH_2 functionalized ligands of cysteamine decrease the overpotential by 0.3 V at 1 mA cm^{-2}, endowing the Ag NPs with 53-fold enhanced TOF and 9.3-fold increased FE for CO (reaching 93%) at −0.6 V vs RHE. This finding provides new vista in inorganic material-based catalysis.

■ ASSOCIATED CONTENT

Supporting Information

The Supporting Information is available free of charge on the ACS Publications website at DOI: 10.1021/acs.jpclett.8b00959.

Materials and Methods, Figures S1−S14, and Table S1 (PDF)

■ AUTHOR INFORMATION

Corresponding Authors

*E-mail: wangzhijiang@hit.edu.cn.
*E-mail: tcheng@caltech.edu.
*E-mail: wag@wag.caltech.edu.

ORCID

Zhijiang Wang: 0000-0001-9314-7922
Kun Sun: 0000-0003-0457-5437
Tao Cheng: 0000-0003-4830-177X
William A. Goddard III: 0000-0003-0097-5716

Notes

The authors declare no competing financial interest.

■ ACKNOWLEDGMENTS

T.C. and W.A.G. were supported by the Joint Center for Artificial Photosynthesis, a DOE Energy Innovation Hub, supported through the Office of Science of the U.S. Department of Energy under Award No. DE-SC0004993. This work used the Extreme Science and Engineering Discovery Environment (XSEDE), which is supported by National Science Foundation Grant Number ACI-1053575. Z.W. acknowledges financial support from the Open Project of State Key Laboratory of Urban Water Resource and Environment, Harbin Institute of Technology (No. HC201813). L.W. acknowledges financial support from the National Natural Science Foundation of China (No. 81771903) and Wuliande Foundation of Harbin Medical University (No. WLD-QN1404).

■ REFERENCES

(1) Olah, G. A.; Prakash, G. K. S.; Goeppert, A. Anthropogenic Chemical Carbon Cycle for a Sustainable Future. *J. Am. Chem. Soc.* **2011**, *133*, 12881−12898.

(2) Feldman, D. R.; Collins, W. D.; Gero, P. J.; Torn, M. S.; Mlawer, E. J.; Shippert, T. R. Observational determination of surface radiative forcing by CO_2 from 2000 to 2010. *Nature* **2015**, *519*, 339−343.

(3) Rosen, B. A.; Salehi-Khojin, A.; Thorson, M. R.; Zhu, W.; Whipple, D. T.; Kenis, P. J. A.; Masel, R. I. Ionic Liquid−Mediated Selective Conversion of CO_2 to CO at Low Overpotentials. *Science* **2011**, *334*, 643−644.

(4) Benson, E. E.; Kubiak, C. P.; Sathrum, A. J.; Smieja, J. M. Electrocatalytic and homogeneous approaches to conversion of CO_2 to liquid fuels. *Chem. Soc. Rev.* **2009**, *38*, 89−99.

(5) Kondratenko, E. V.; Mul, G.; Baltrusaitis, J.; Larrazabal, G. O.; Perez-Ramirez, J. Status and perspectives of CO_2 conversion into fuels and chemicals by catalytic, photocatalytic and electrocatalytic processes. *Energy Environ. Sci.* **2013**, *6*, 3112−3135.

(6) Kuhl, K. P.; Hatsukade, T.; Cave, E. R.; Abram, D. N.; Kibsgaard, J.; Jaramillo, T. F. Electrocatalytic Conversion of Carbon Dioxide to Methane and Methanol on Transition Metal Surfaces. *J. Am. Chem. Soc.* **2014**, *136*, 14107−14113.

(7) Ong, W.-J.; Putri, L. K.; Tan, Y.-C.; Tan, L.-L.; Li, N.; Ng, Y. H.; Wen, X.; Chai, S.-P. Unravelling charge carrier dynamics in protonated g-C_3N_4 interfaced with carbon nanodots as co-catalysts toward enhanced photocatalytic CO_2 reduction: A combined experimental and first-principles DFT study. *Nano Res.* **2017**, *10*, 1673−1696.

(8) Zhang, X.; Zhang, Z.; Li, J.; Zhao, X.; Wu, D.; Zhou, Z. Ti_2CO_2 MXene: a highly active and selective photocatalyst for CO_2 reduction. *J. Mater. Chem. A* **2017**, *5*, 12899−12903.

(9) Li, N.; Chen, X.; Ong, W.-J.; MacFarlane, D. R.; Zhao, X.; Cheetham, A. K.; Sun, C. Understanding of Electrochemical Mechanisms for CO_2 Capture and Conversion into Hydrocarbon Fuels in Transition-Metal Carbides (MXenes). *ACS Nano* **2017**, *11*, 10825−10833.

(10) Qiao, J.; Liu, Y.; Hong, F.; Zhang, J. A review of catalysts for the electroreduction of carbon dioxide to produce low-carbon fuels. *Chem. Soc. Rev.* **2014**, *43*, 631−675.

(11) Kondratenko, E. V.; Mul, G.; Baltrusaitis, J.; Larrazábal, G. O.; Pérez-Ramírez, J. Status and perspectives of CO_2 conversion into fuels and chemicals by catalytic, photocatalytic and electrocatalytic processes. *Energy Environ. Sci.* **2013**, *6*, 3112−3135.

(12) Liu, M.; Pang, Y.; Zhang, B.; De Luna, P.; Voznyy, O.; Xu, J.; Zheng, X.; Dinh, C. T.; Fan, F.; Cao, C.; de Arquer, F. P. G.; Safaei, T. S.; Mepham, A.; Klinkova, A.; Kumacheva, E.; Filleter, T.; Sinton, D.; Kelley, S. O.; Sargent, E. H. Enhanced electrocatalytic CO_2 reduction via field-induced reagent concentration. *Nature* **2016**, *537*, 382−386.

(13) Kim, D.; Resasco, J.; Yu, Y.; Asiri, A. M.; Yang, P. Synergistic geometric and electronic effects for electrochemical reduction of carbon dioxide using gold−copper bimetallic nanoparticles. *Nat. Commun.* **2014**, *5*, 4948.

(14) Lu, Q.; Rosen, J.; Zhou, Y.; Hutchings, G. S.; Kimmel, Y. C.; Chen, J. G.; Jiao, F. A selective and efficient electrocatalyst for carbon dioxide reduction. *Nat. Commun.* **2014**, *5*, 3242.

(15) Zhu, W.; Michalsky, R.; Metin, Ö.; Lv, H.; Guo, S.; Wright, C. J.; Sun, X.; Peterson, A. A.; Sun, S. Monodisperse Au Nanoparticles for Selective Electrocatalytic Reduction of CO_2 to CO. *J. Am. Chem. Soc.* **2013**, *135*, 16833−16836.

(16) Kim, C.; Jeon, H. S.; Eom, T.; Jee, M. S.; Kim, H.; Friend, C. M.; Min, B. K.; Hwang, Y. J. Achieving Selective and Efficient Electrocatalytic Activity for CO_2 Reduction Using Immobilized Silver Nanoparticles. *J. Am. Chem. Soc.* **2015**, *137*, 13844−13850.

(17) Fang, Y.; Flake, J. C. Electrochemical Reduction of CO_2 at Functionalized Au Electrodes. *J. Am. Chem. Soc.* **2017**, *139*, 3399−3405.

(18) Tornow, C. E.; Thorson, M. R.; Ma, S.; Gewirth, A. A.; Kenis, P. J. A. Nitrogen-Based Catalysts for the Electrochemical Reduction of CO_2 to CO. *J. Am. Chem. Soc.* **2012**, *134*, 19520−19523.

(19) Rosen, B. A.; Haan, J. L.; Mukherjee, P.; Braunschweig, B.; Zhu, W.; Salehi-Khojin, A.; Dlott, D. D.; Masel, R. I. In Situ Spectroscopic Examination of a Low Overpotential Pathway for Carbon Dioxide Conversion to Carbon Monoxide. *J. Phys. Chem. C* **2012**, *116*, 15307−15312.

(20) Lu, Q.; Jiao, F. Electrochemical CO_2 reduction: Electrocatalyst, reaction mechanism, and process engineering. *Nano Energy* **2016**, *29*, 439−456.

(21) Sun, K.; Cheng, T.; Wu, L.; Hu, Y.; Zhou, J.; Maclennan, A.; Jiang, Z.; Gao, Y.; Goddard, W. A.; Wang, Z. Ultrahigh Mass Activity for Carbon Dioxide Reduction Enabled by Gold−Iron Core−Shell Nanoparticles. *J. Am. Chem. Soc.* **2017**, *139*, 15608−15611.

(22) Liu, S.; Tao, H.; Zeng, L.; Liu, Q.; Xu, Z.; Liu, Q.; Luo, J.-L. Shape-Dependent Electrocatalytic Reduction of CO_2 to CO on Triangular Silver Nanoplates. *J. Am. Chem. Soc.* **2017**, *139*, 2160−2163.

(23) Can, M.; Armstrong, F. A.; Ragsdale, S. W. Structure, Function, and Mechanism of the Nickel Metalloenzymes, CO Dehydrogenase, and Acetyl-CoA Synthase. *Chem. Rev.* **2014**, *114*, 4149−4174.

(24) Hansen, H. A.; Varley, J. B.; Peterson, A. A.; Nørskov, J. K. Understanding Trends in the Electrocatalytic Activity of Metals and Enzymes for CO_2 Reduction to CO. *J. Phys. Chem. Lett.* **2013**, *4*, 388−392.

(25) Cheng, T.; Xiao, H.; Goddard, W. A. Reaction Mechanisms for the Electrochemical Reduction of CO2 to CO and Formate on the Cu(100) Surface at 298 K from Quantum Mechanics Free Energy Calculations with Explicit Water. *J. Am. Chem. Soc.* **2016**, *138*, 13802−13805.

(26) Cheng, T.; Xiao, H.; Goddard, W. A. Nature of the Active Sites for CO Reduction on Copper Nanoparticles; Suggestions for Optimizing Performance. *J. Am. Chem. Soc.* **2017**, *139*, 11642−11645.

(27) Michota, A.; Kudelski, A.; Bukowska, J. Influence of electrolytes on the structure of cysteamine monolayer on silver studied by surface-enhanced Raman scattering. *J. Raman Spectrosc.* **2001**, *32*, 345−350.

(28) Kudelski, A. Structures of monolayers formed from different HS—$(CH_2)_2$—X thiols on gold, silver and copper: comparitive studies by surface-enhanced Raman scattering. *J. Raman Spectrosc.* **2003**, *34*, 853−862.

(29) Kudelski, A.; Hill, W. Raman Study on the Structure of Cysteamine Monolayers on Silver. *Langmuir* **1999**, *15*, 3162−3168.

(30) Schmitt, K. G.; Gewirth, A. A. In Situ Surface-Enhanced Raman Spectroscopy of the Electrochemical Reduction of Carbon Dioxide on Silver with 3,5-Diamino-1,2,4-Triazole. *J. Phys. Chem. C* **2014**, *118*, 17567−17576.

(31) Fenner, W. R.; Hyatt, H. A.; Kellam, J. M.; Porto, S. P. S. Raman cross section of some simple gases. *J. Opt. Soc. Am.* **1973**, *63*, 73−77.

(32) Kameneva, S. V.; Tyurin, D. A.; Nuzhdin, K. B.; Feldman, V. I. Matrix isolation and ab initio study on HCN/CO_2 system and its radiation-induced transformations: Spectroscopic evidence for HCN··· CO_2 and trans-HCNH···CO_2 complexes. *J. Chem. Phys.* **2016**, *145*, 214309.

(33) Hsieh, Y.-C.; Senanayake, S. D.; Zhang, Y.; Xu, W.; Polyansky, D. E. Effect of Chloride Anions on the Synthesis and Enhanced Catalytic Activity of Silver Nanocoral Electrodes for CO_2 Electroreduction. *ACS Catal.* **2015**, *5*, 5349−5356.

DOI: 10.1021/acs.jpclett.8b00959
J. Phys. Chem. Lett. 2018, 9, 3057−3061